Chapter III Volcanic Activity of Talang and Sinabung volcanoes

This chapter describes the tectonic setting and the geological structure of Sumatra and volcanic activity as main factor especially the level of activity when tectonic earthquakes occur and trigger an increase in volcanic activity. Many evidences indicate increase in activity under certain conditions that the stress changes caused by a large earthquake could trigger volcanic eruptions. Previous researchers show that triggering thresholds of stress change vary from system to system, for example, peak dynamic stresses were 0.1 MPa at Augustine volcano, whereas peak dynamic stresses were less than 0.1 MPa at other North American sites (Prejean, 2004). Volcanoes will response to tectonic earthquakes in different way. The response related with the characteristic of the volcanic activity, and the triggering mechanism depends on recent activity and geological condition of the volcanoes. For example, Moran (2003) suggests that the magmatic-hydrothermal systems beneath the Katmai volcanoes are fundamentally different than those at other Alaskan volcanoes which are not triggered. The suggestion based on occurrence of triggered earthquakes at Katmai volcanoes but short-term triggering was absence at other Alaskan volcanoes.

One of the important methods to make clear mechanisms of triggering is integrated monitoring of volcanoes. In this chapter, the volcanic activity of Talang and Sinabung will be described to show the levels of activity before and during the triggering process. A combination of seismicity and deformation measurements may be able to reveal the triggering processes that lead to eruption. Earthquake swarm is a common precursor of eruptions and may trigger further unrest in a volcanic system (Manga & Brodsly, 2008). Increase in seismicity of volcano is reflected as increase in number and energy, change in frequencies and focal mechanism. Volcanic deformation are induced by magma ascent and discharge. Rising magma flow through cracks or conduits in which then accumulated in reservoirs, changing pressure on the source, conduit, and the surrounding area. This is detected as ground deformation on the surface of volcano. The pattern and rate of surface deformation around volcanoes reflect the tectonic and volcanic processes transmitted to the surface through elastic deformation of the crust. Volcanic body

deformed by inflating, deflating, and growing bodies of various shapes and sizes, the opening or closing of a cavity or crack; such as a strike–slip or dip–slip fault, and composite sources that include both tensile and shear movements.

III.1 Talang Volcanic Activity

III.1.1 Geological Setting

Talang volcano is one of the active volcanoes in Indonesia, located at West Sumatra (Figure III.1). Sumatra, tectonically active region, is characterized by a great number of earthquakes on the subducting Indo-Australia Plate, Sumatra Fault Zone and active volcanoes lined up along the fault zone. Volcanic eruptions and increase in volcanic activity are sometimes related with tectonic earthquakes.

Geologically, the two peaks of Talang volcano lies in an ellipsoid-shaped pattern associated with depression zone on southeastern part of Sumani segment of the Great Sumatra Fault (Sieh, 2000, Figure III.2). Genrich et al. in Sieh (2000) showed that strain rate during the early 1990 is consistent with a velocity of 23 ± 5 mm/year of plate movement.

The zone of depression is most likely formed due to fault/fracture (Purbawinata et al, 2005). The presence of cracks on the slopes of Talang Lake and alignment of several fumaroles indicate that the activity of Talang volcano is affected by geological structure. The detail of the geological map of Talang volcano shows a normal faulting across the volcano body in southeast – northwest direction between Talang Jantan and Talang Batino as shown in Figure III.3.

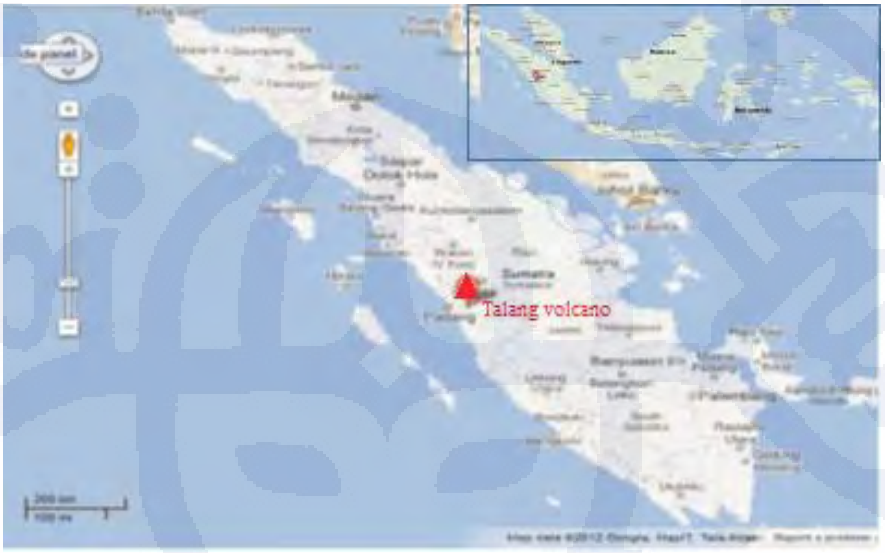

Figure III.1. Location of Talang volcano is denoted by red triangle.

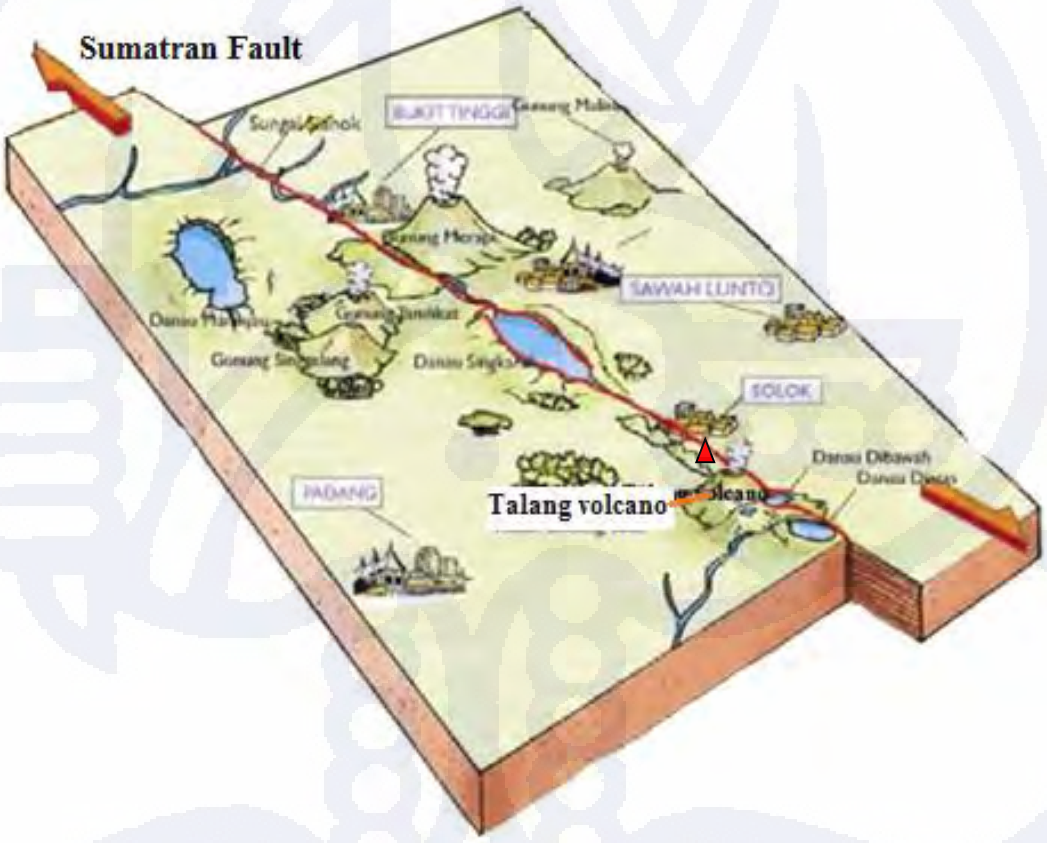

Figure III.2. Sumatra Fault in western Sumatra where Talang volcano located on southeastern Sumani segment. (modified from Sieh and Natawidjaja, 2000, the picture is taken from the brochure: Sumatra Earthquake Prone, LIPI - Caltech). The location of Talang volcano is denoted by red triangular.

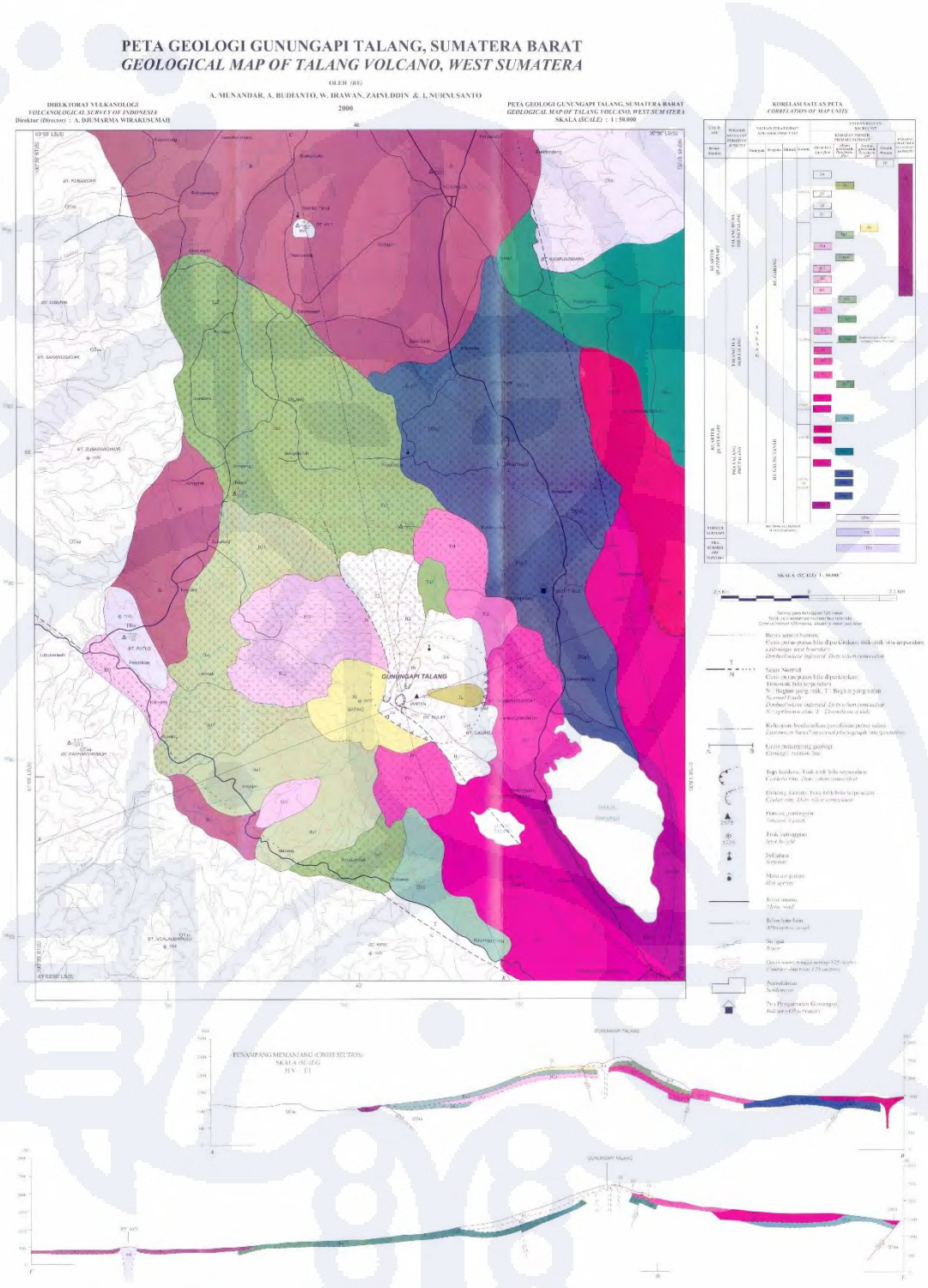

Figure III.3. Geological map of Talang volcano. There is a lineament cross the volcano in west-east direction (Source: Munandar, 2000)

III.1.2 Seismic activity

Eruptive activity of Talang volcano has a long history with the shortest interval of 2 years and the longest 40 years. In the historical record, the VEI2 magmatic eruptions occurred in 1833, 1843, and 1845. After the 1845 eruption, volcanic eruptions were merely phreatic type and were not followed by a magmatic eruption. They were recorded in 1963, 1967, 1972, 1980-1981, 2001, 2003, 2005, 2006, and 2007 (Kriswati, 2010). Several centers of eruption are identified in Talang volcano, these are the Talang crater, South crater, Kepundan Panjang, Gabuo Atas, Gabuo Bawah, and Batu Bajanjang spring. The phreatic eruption on April 12th 2005 occurred in the South crater, preceded by increase in earthquake number 2 days before. Similar increase in seismicity was recorded on September 30th and October 1st, 2009 after Southern Sumatra earthquakes, with magnitude 7.6 and 6.6 respectively, height of ash emmision increased on October 1st, 2009.

Seismic events at Talang volcano are classified into 2 tectonic types of regional (TJ) and local earthquake (TL) and 4 volcanic types; these are deep volcanic quake type-VA (>1 km beneath the volcano), shallow volcanic quake type-VB (<1 km), tremor, and low frequency quake. In 2004, the seismicity of Talang volcano remained low (Figure III.4). The numbers of type-VA, VB, and tremor events increased in first week of April 2005, followed by a phreatic eruption on April 12th 2005. Increase in seismicity repeated in several times until 2013.

The hypocenter of VA earthquakes are located by using Geiger Adaptive Damping (GAD) method (Nishi, 2005). Seismic data were recorded by temporary 4 digital and one permanent seismographs during the periods of December 2007 (Figure III.5), February – March 2008 (Figure III.6), July – August 2009 (Figure III.7), August – September 2009 (Figure III.8), and October 2009 (Figure III.9) Focal mechanism of VA earthquakes with S-P arrival time less than 4 second was determined. A grid search method was used to fit amplitude and polarity of P-wave first motion, assuming a double couple mechanism and homogenous half space medium (Hidayati, 2008). The focal mechanisms of events are consist of normal, reverse, and strike-slip type. Table III.1 shows the dominant mechanism and depth of VA earthquakes.

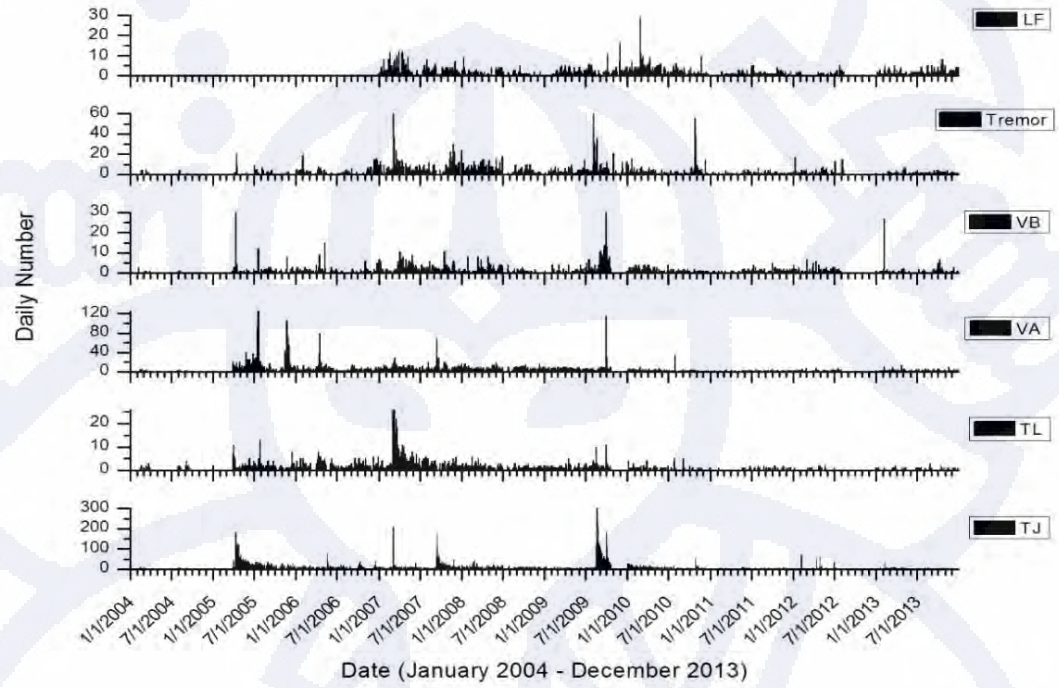

Figure III.4. Daily numbers of types of events in the period of January 2004 – December 2013.

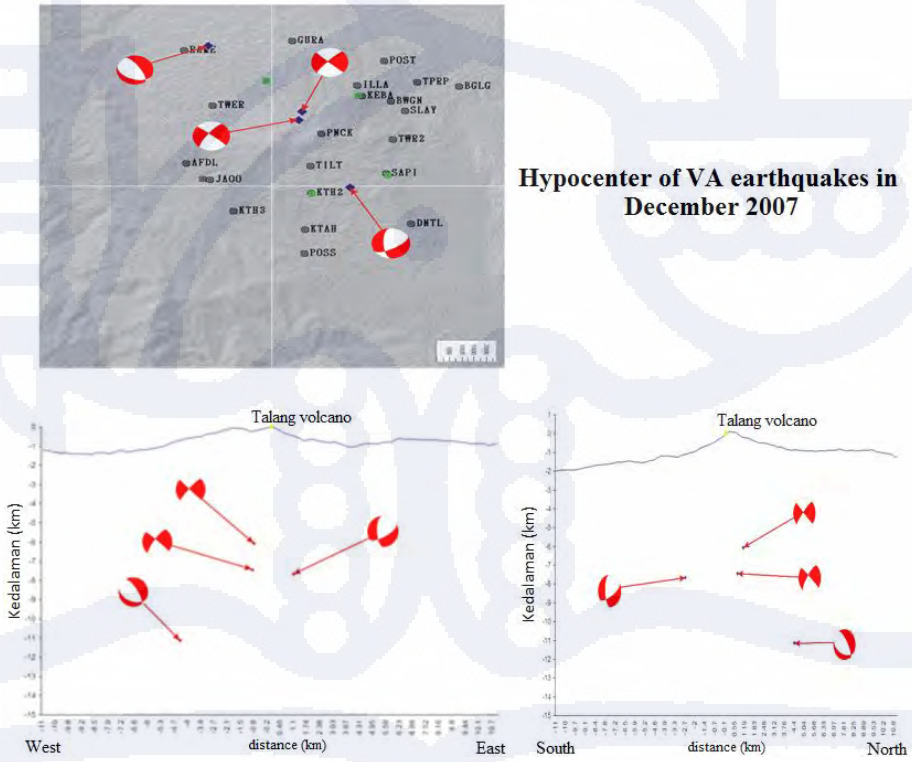

Figure III.5. Distribution of hypocenters and focal mechanism in December 2007 (Source: Hidayati, 2007)

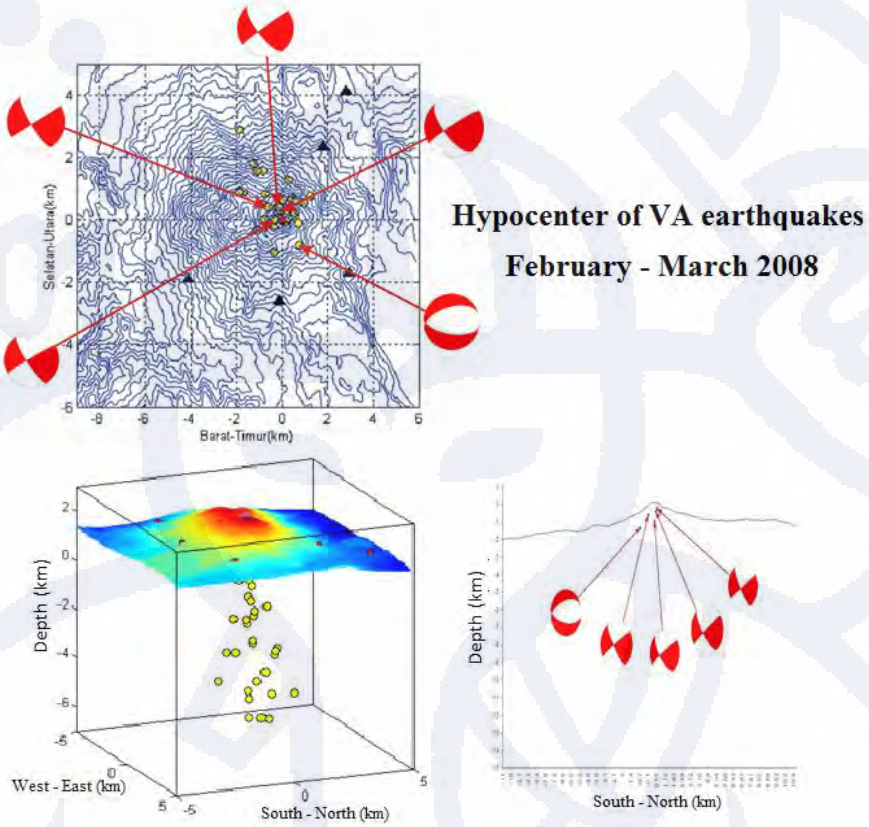

Figure III.6. Distribution of hypocenters and focal mechanism in February-March 2008 (Source: Mulyana, 2008).

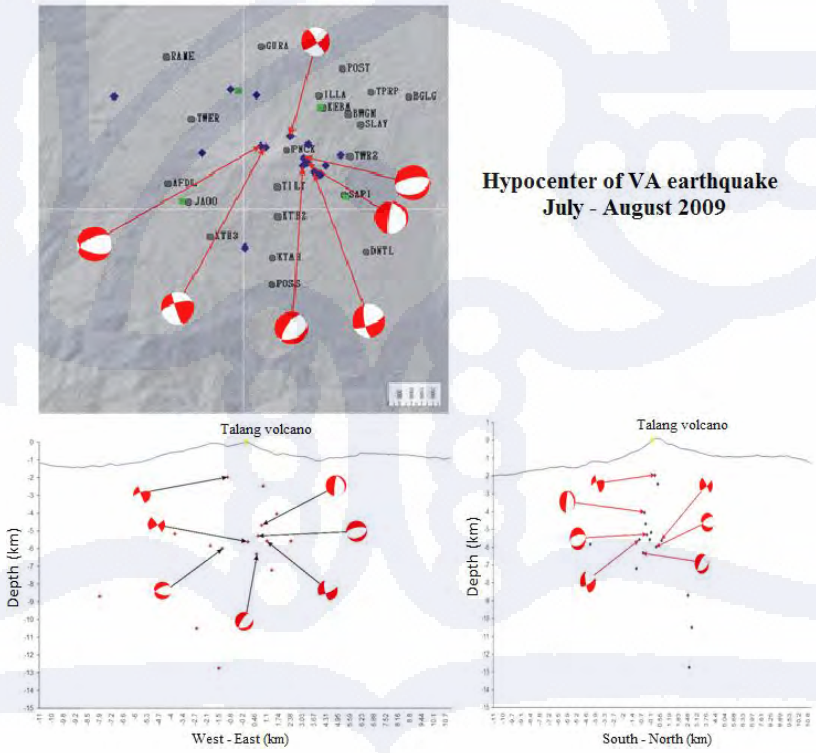

Figure III.7 Distribution of hypocenters and focal mechanism in July-August 2009

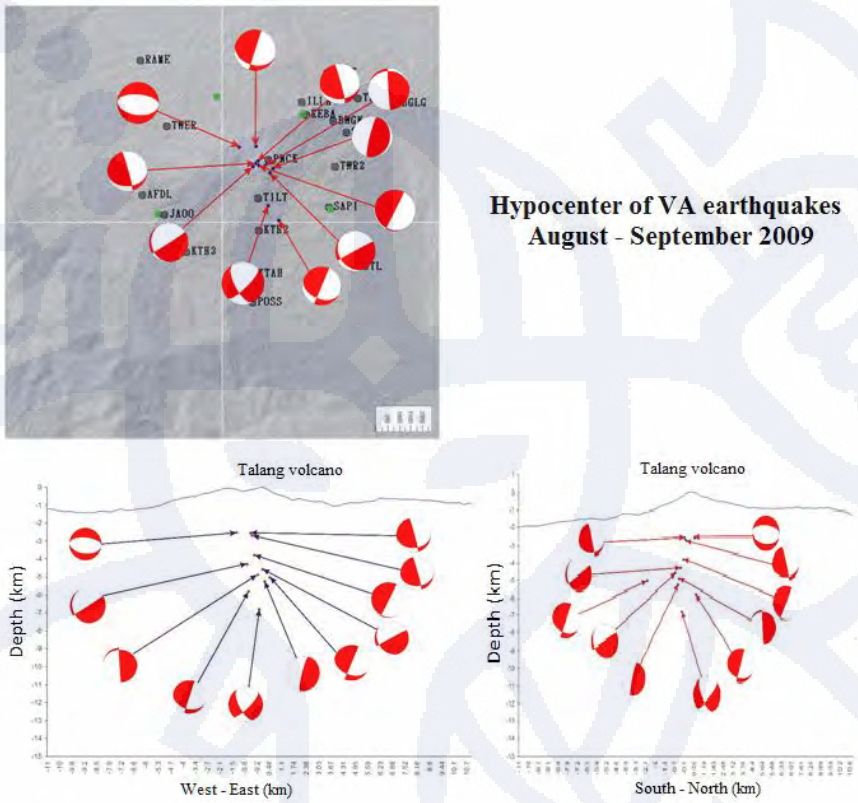

Figure III.8. Distribution of hypocenters and focal mechanism in August-September 2009

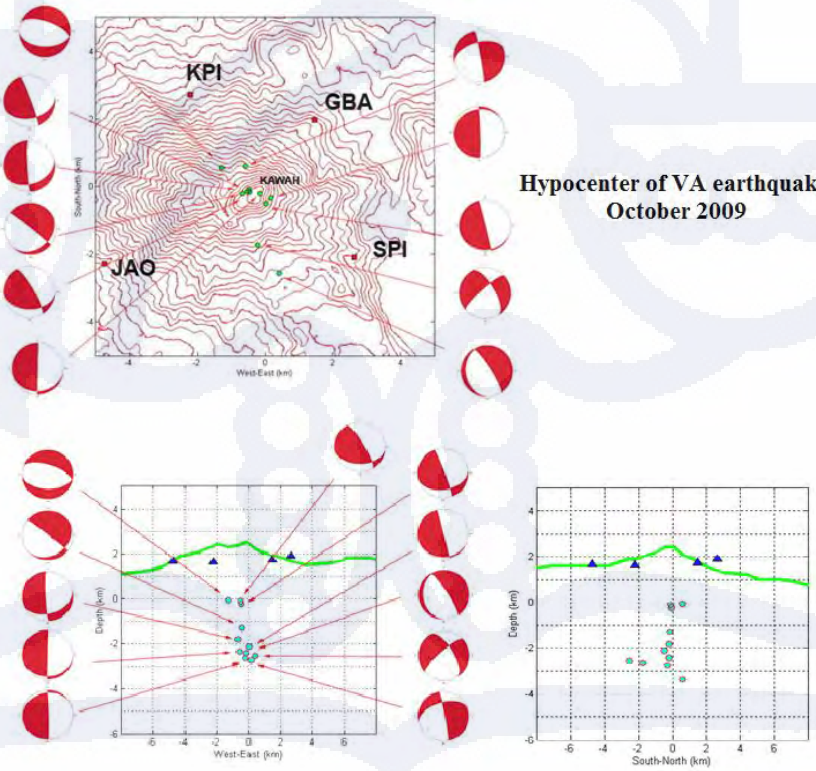

Figure III.9. Distribution of hypocenters and focal mechanism in October 2009

Table III.1. The resume of focal mechanism of Talang volcanic earthquake in some measurement periods

Period	Depth	Dominant Mechanism	Trending
December 2007	2 – 6 km	Strike slip	SE-NW
February – March 2008	2 - 6 km	Strike slip	SE-NW
July – August 2009	2 – 8 km	Strike slip/Normal	SE-NW
August – September 2009	2 – 9 km	Normal	SE-NW
October 2009	2 – 5 km	Normal	SE-NW

Distribution of epicenters in December 2007 showed trending in the direction of southeast-northwest (Hidayati, 2007), and this corresponds to the direction of fault/fracture which cuts the Talang volcano. The focal mechanism in December 2007 consists of strike slip and normal faultings. The strike slip faulting showed extension in east-west direction and contraction in north-south direction. This is consistent with the mechanism and the direction of the Sumatra Fault. In February-March 2008, the epicenter distribution showed a southeast-northwest alignment at a depth of 2-6 km below the summit (Mulyana, 2008). Generally the earthquakes have a similar focal mechanism to the previous period, the same direction with the Sumatra Fault. The hypocenter distribution of July-August 2009 also showed trend in southeast-northwest at depths from 2 to 8 km below the summit, consist of strike slip and normal faults. In the period of August-September 2009, the epicenter were distributed along southeast-northwest alignment at depths 2-9 km below the summit with strike slip and normal faults mechanism. The epicenter distribution in October 2009 oriented southeast-northwest with depths ranging from 2-5 km below the summit. There are earthquakes with reverse fault mechanism accompanying the strike slip and normal faults. Strike slip of VA earthquakes coincide with tectonic stress of Sumatra Fault, it appears that seismic activity at Talang volcano is dominated by the movement of the local structures that are affected by regional tectonic. Considering the compressional stress of Sumatra Fault is in N-S direction, the presence of normal fault of VA earthquakes in 2009 is curious. This is not affected by regional tectonic stress and most likely caused by volcanic activity.

III.1.3 Talang Volcano Deformation

I use GPS campaign data around Talang volcano in 2007 to 2009 to obtain horizontal displacements. The campaign measurement were conducted at 19 points around Talang volcano (Figure III.10) recorded by dual frequency Leica GPS 1200 series for 4-12 hours.

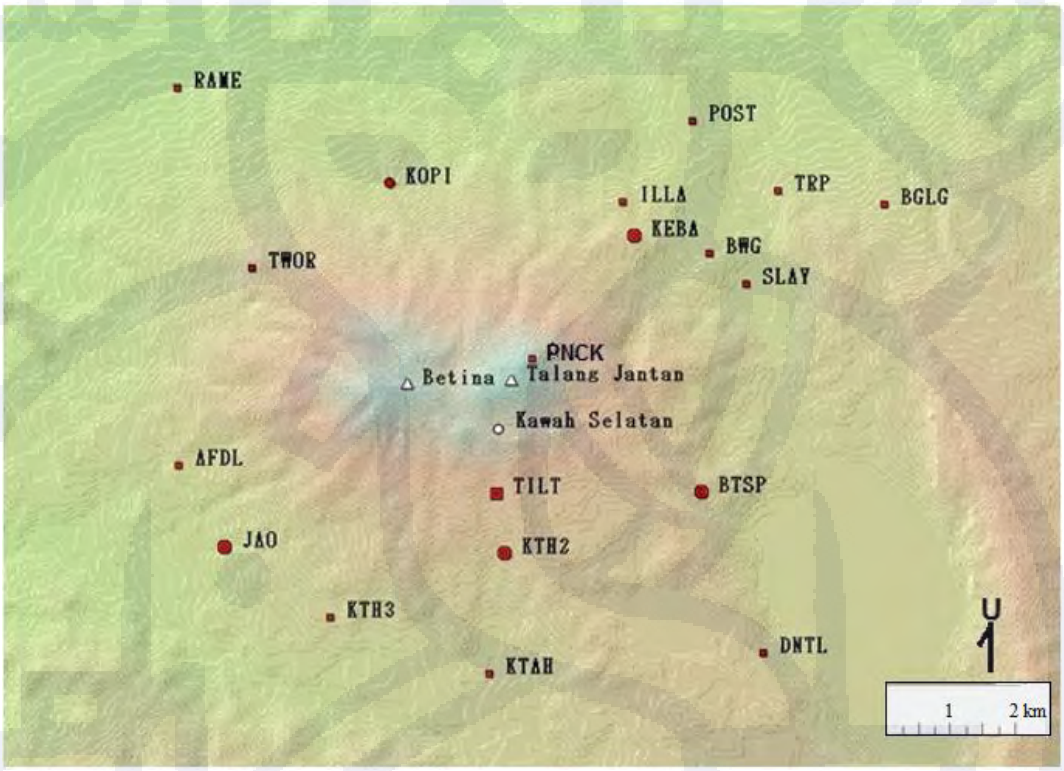

Figure III.10. Distribution of GPS benchmarks in Talang volcano

To determine the pressure source of Talang volcano deformation, the Mogi point source model was applied. Kiyoo Mogi concluded that geodetically measured elevation change and horizontal displacements associated with eruptions in Japan and Hawaii resulted from inflation and deflation of magma bodies within the volcanoes (Mogi, 1958). Before him Anderson (1936), Mindlin and Cheng (1950), McCann and Wilts (1951), Sen (1951), and Yamakawa (1955) had already propose similar models and calculated surface ground deformation caused by a spherical source in an homogeneous semi-infinite elastic crust. Simplification of Yamakawa formulation by Mogi model causes the method to be most widely used to for model surface deformation from a deflating or inflating magma chamber. Mogi (1958) applied his model to the ground deformation associated with the 1914 Sakurajima

eruption and estimated the location of the pressure source. When a Poisson solid is assumed as λ = μ (λ, μ: Lame's constant) the horizontal displacement Δd and the vertical one Δh at the surface with a horizontal distance from the source d caused by a spherical pressure source at a depth f are expressed as follow:

$$\Delta d = \frac{3a^3 P}{4\mu} \frac{d}{(d^2 + f^2)^{3/2}}, \quad \text{(III.1)}$$

$$\Delta h = \frac{3a^3 P}{4\mu} \frac{f}{(d^2 + f^2)^{3/2}}, \quad \text{(III.2)}$$

where μ, a, and P denotes rigidity, radius of the spherical source, and change of the hydro-static pressure in the source, respectively. And for volume change:

$$\Delta V_p = 1.33\pi \cdot k$$

The 2007 – 2009 deformation which is analyzed as a time series showed inflation at the southern slope of Talang volcano at a depth of 3 kilometers, defined as an increase in pressure in the body of Talang volcano (Figure III.11). The volume change is approximately 2 million m^3/year (Kriswati, 2013). Accumulation of energy that triggers an increase in volcanic activity takes a long time to have enough pressure to push fluid to the surface and generate an inflation in Talang volcano body.

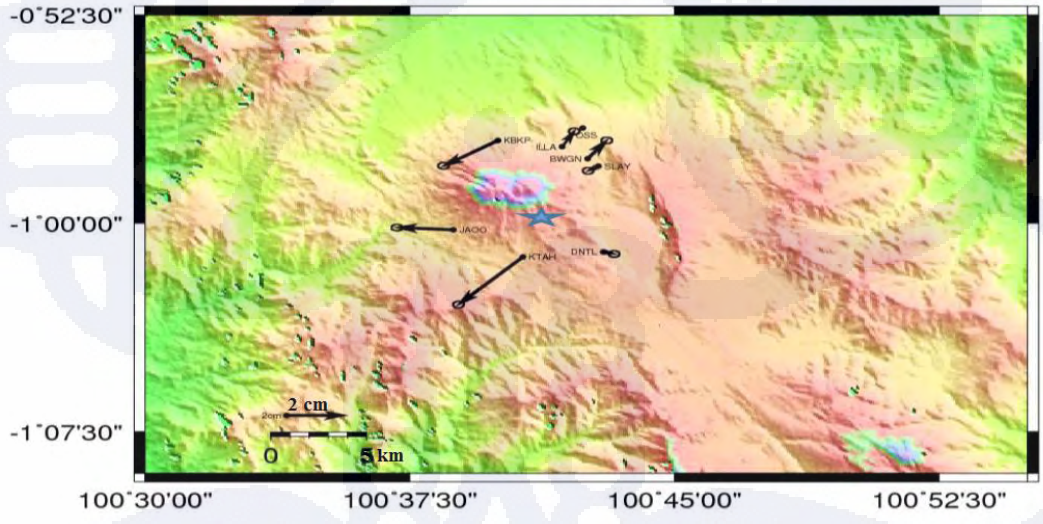

Figure III.11. Inflation in southern slope of Talang volcano, is shown by GPS velocity vector in the period of 2007-2009 that has radial pattern away from the western crater (Kriswati, 2013). A star denotes Mogi poin source determine from GPS data.

In the short period, July-August 2009 horizontal displacement data and applied Okada model to explain the deformation of Talang volcano show an oblique fault zone (dextral and reverse fault) that cuts the top of Talang volcanic area (Kriswati, 2013, Figure III.12).

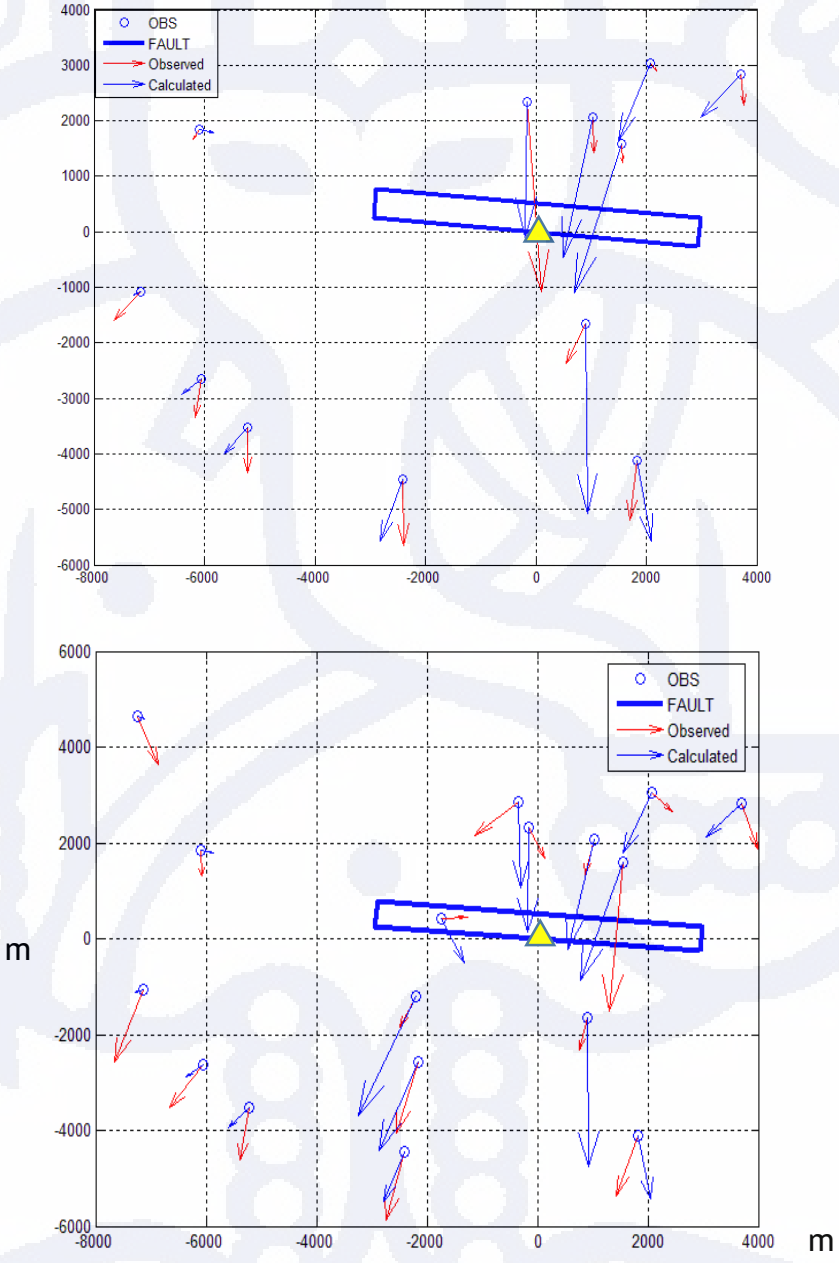

Figure III.12. Horizontal displacement of July – August 2009 period (up) and July – October 2009 period (bottom). The fault model is obtained using the formulations of Okada (1985) for surface displacements due to dislocations in an elastic half-space.The yellow triangle is Talang location. The depth of fault is 3 – 6 km.

III.1.4 Model of Talang Volcanic Activity

Parameters of the fault derived from deformation data is correspond to the pattern of epicenter distribution which trending southeast - northwest. Fault mechanism of deformation data also showed a similar pattern to focal mechanism of volcanic earthquakes recorded at Talang volcano in the period 2007 to 2009 (Kriswati, 2010). Sumatran fault has a right lateral mechanism trending southeast - northwest. Those data show that the activity of seismicity and deformation in Talang volcano are dominated by the movement of local structures that are affected by the movement of local structures due to regional tectonic movements of the right lateral Sumatran fault. Based on the data, the pressure sources model of Talang volcanic activity has been proposed as illustrated in Figure III.13. The model show two sources, there are point source in shallow part beneath southern crater (based on 2007-2009 data) and a fault beneath the main crater (based on July – August and October 2009 data). The relation between the two sources is still unknown.

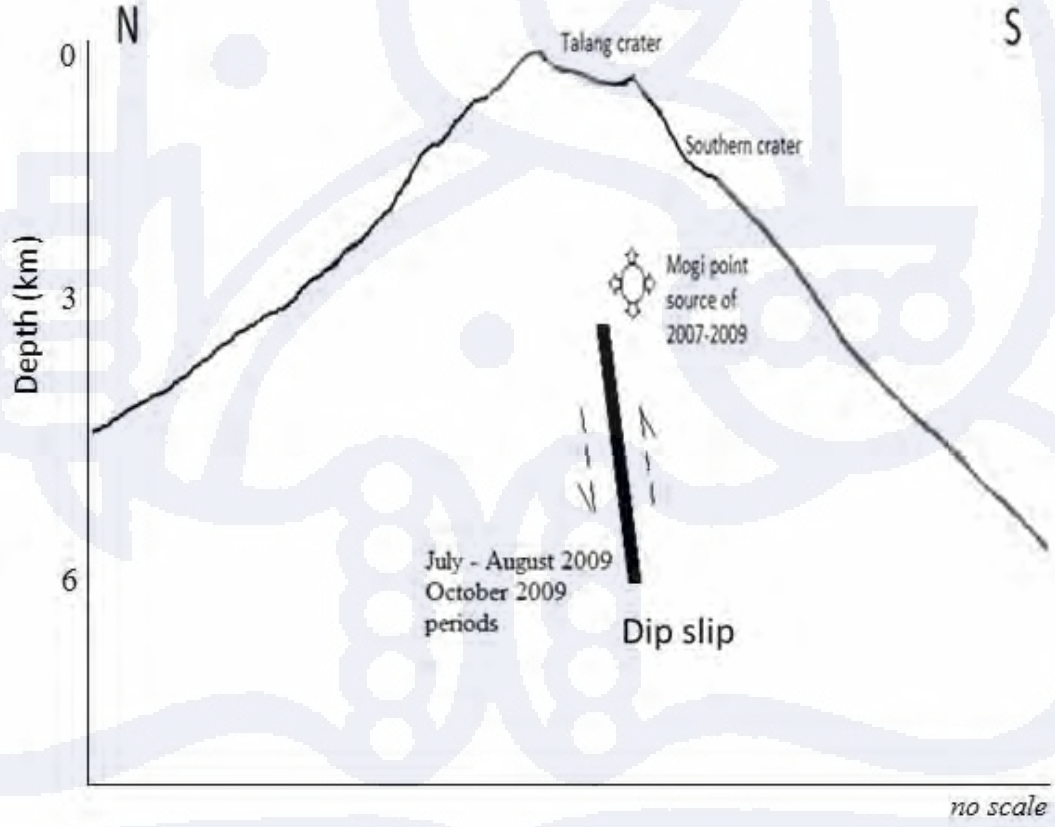

Figure III.13. The simple model for the pressure source in Talang volcano.

III.2 Sinabung Volcanic Activity

III.2.1 Geological Setting

The Sinabung volcano is located at the northern part of the dextral strike-slip Sumatran Fault and included in Toba caldera volcanic cluster (Muraoka, 2010). A geomorphological study of Sieh and Natawidjaja (2000) revealed that the Sumatran Fault is partitioned into 19 major sections, mostly caused by the changes in the rate and direction of the Indo-Australian plate motion along Sumatra. The slip rate is larger in northwestern Sumatra by 24 mm/yr and smaller in southeastern Sumatra by 6 mm/yr (McCaffrey, 1991; Bellier and Sébrier, 1995; Genrich et al., 2000; McCaffrey et al., 2000; Prawirodirdjo et al., 2000). This segmentation is characterized by thirteen pull-apart basins caused by dilatational step-overs and one pressure ridge (Muraoka, 2010). Almost all the pull-apart basins along the Sumatran fault occur near the clustered volcanoes, but rarely inside of the areas (Figure III.14, upper). There are two contradictory roles of the volcanic clusters in the formation of pull-apart basins; the volcanic clusters macroscopically play a role of generators to pull-apart basins along the Sumatran fault which is typically observed in northwestern Sumatra and the areas of the volcanic clusters themselves are inhibitors to pull-apart basins that is observed in the large volcanic cluster areas such as Toba caldera volcanic cluster where pull-apart basins are missing for 150 km along the Sumatran fault from 2.1ºN to 3.2ºN. Sinabung volcano occupies the northwestern edge of the Toba caldera volcanic cluster (Figure III.14, bottom). Sinabung volcano geologically located on faulting zone. The fault plane strike in the direction N30°/N210° crossing the summit of the volcano (Figure III.15).

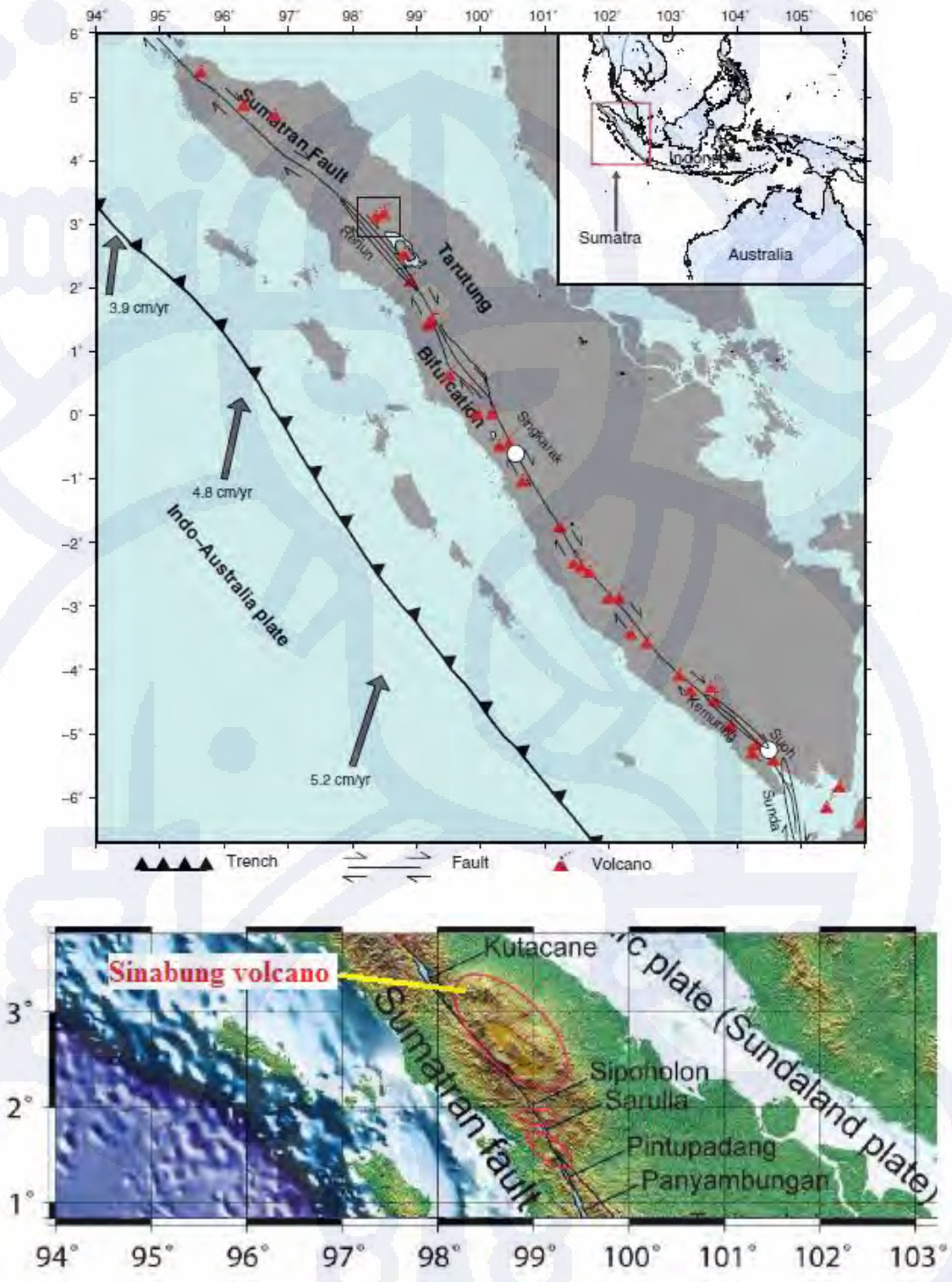

Figure III.14 Regional tectonic setting of Sumatra and Sinabung volcano (box) (Muksin, 2014, upper). Sinabung volcano location in Toba Caldera volcano cluster (Muraoka, 2010, bottom).

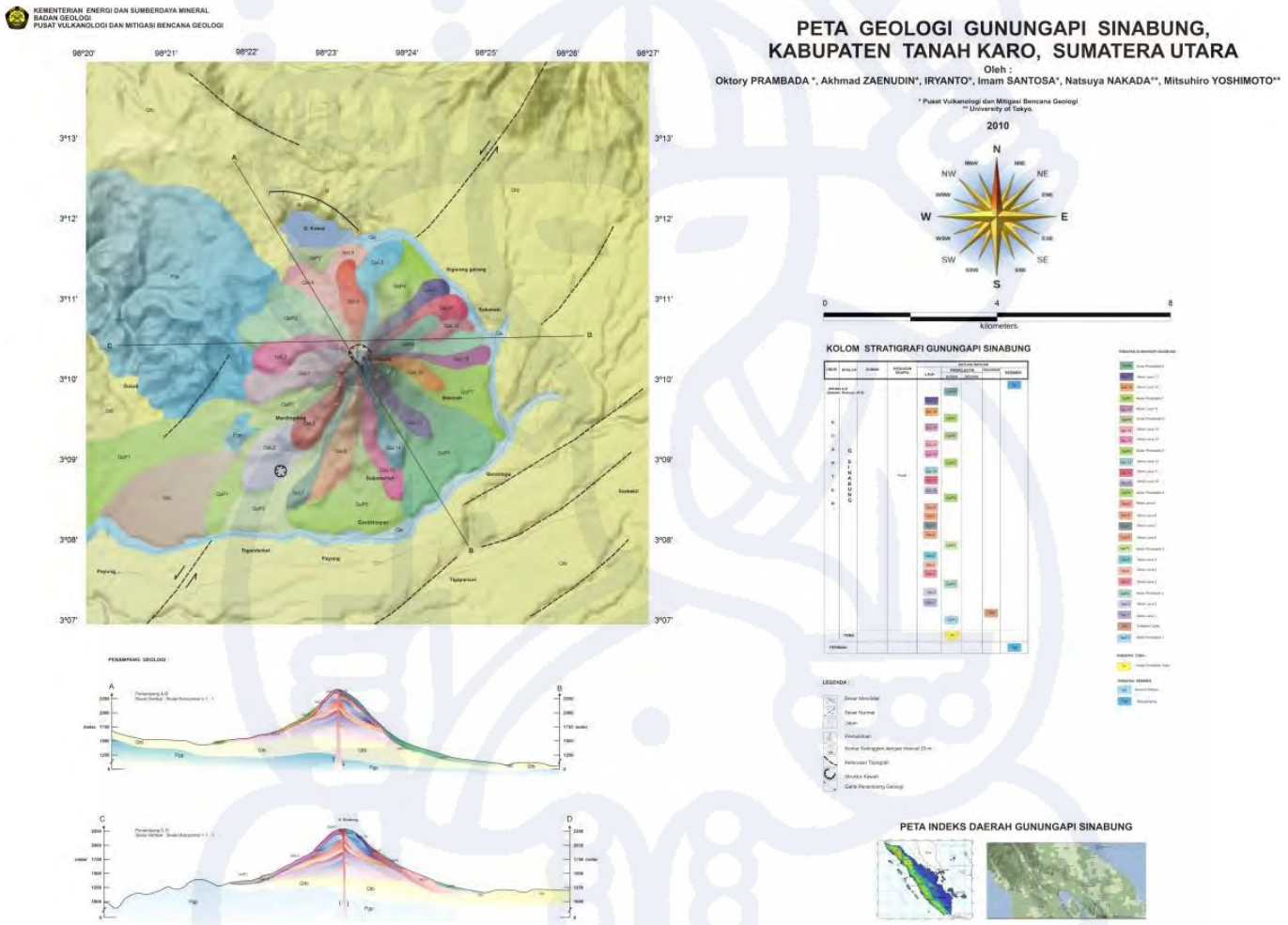

Figure III.15. Geological map of Sinabung volcano (Prambada, 2010)

III.2.2 Seismic activity

Sinabung volcano erupted several times from August 29th to September 7th in 2010. The eruption precursor could not be determined because no monitoring system was installed before the eruption. The volcano entered into a new series of eruptions on September 15, 2013, which was preceded by the increase in number of volcanic earthquakes. Seismic events at Sinabung are classified into 2 tectonic types of regional (TJ) and local earthquake (TL) and 4 volcanic types. Volcanic types are type-VA (>1 km beneath the volcano), type-VB (<1 km), gas emmision, and explosion quakes. Seismicity of Type-VA event fluctuated in a certain range before July 2013 and increased in the periods of August - October 2010, October 2010 - March 2011, January – June 2012, and July – November 2012. The number of type-VA stayed at a low level 1 – 10 events/day, however it suddenly increased to 32 events on July 4th, 2013 and reached at a peak of 129 events 2 days after (Figure III.16). Such high seismicity was followed by the start of the new series of eruptions on September 15th, 2013.

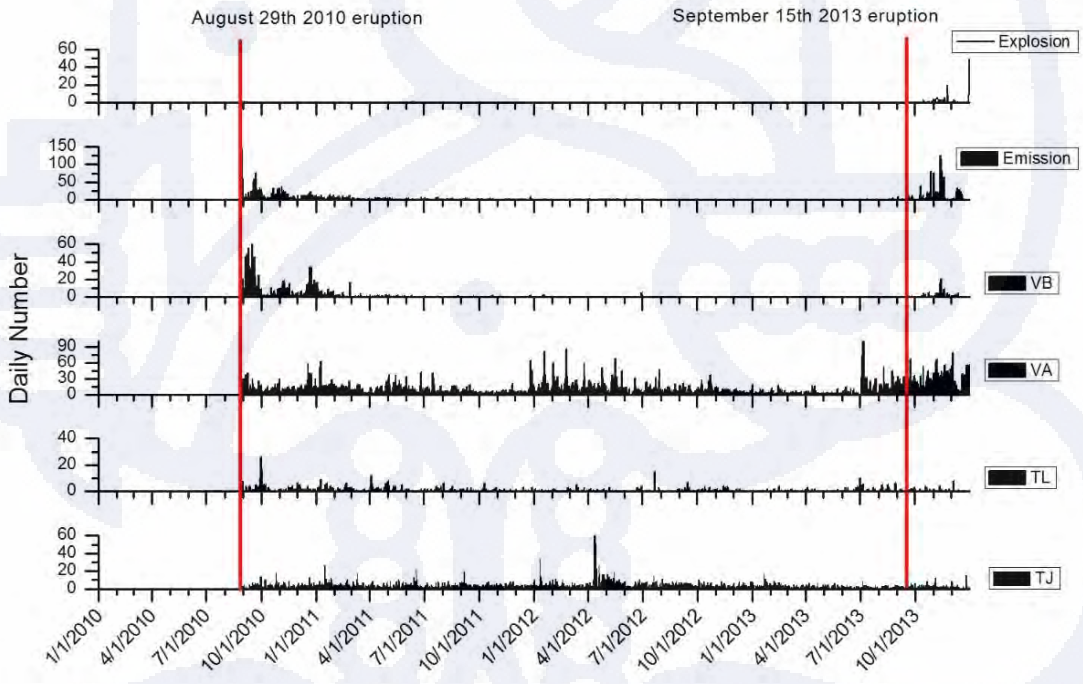

Figure III.16. The daily number of earthquakes which are recorded in Sinabung volcano. TJ: regional tectonic earthquake, TL: local tectonic, VB: shallow volcanic earthquake and VA: deep one. Daily numbers began to be counted after the eruption on August 29th, 2010. The red lines are beginning of 2010 and 2013 eruption respectively.

In October 2010 – July 2013, the hypocenter of VT earthquakes of Sinabung volcano is distributed in the radius of 10 km from summit and in the depth 0 - 35 km beneath the summit (Indrastuti, 2014). The hypocenter is located using Geiger Adaptive Damping (GAD) method (Nishi, 2005) with 6 layers velocity structure which best fitted for Sinabung volcano area. The layers taken from seismic velocity derived from the Vp and Vp/Vs tomography study (Indrastuti, 2014). Compare to May and June hypocenter, there are a shifting of earthquakes distribution in July 2013. In July 2013 the hypocenters are clustered beneath the summit and reached the depth of 8 km (Figure III.17).

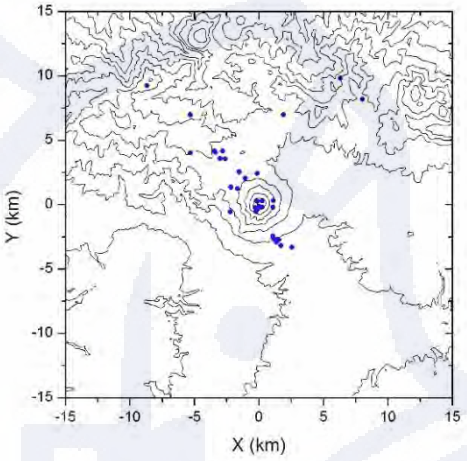

May 2013

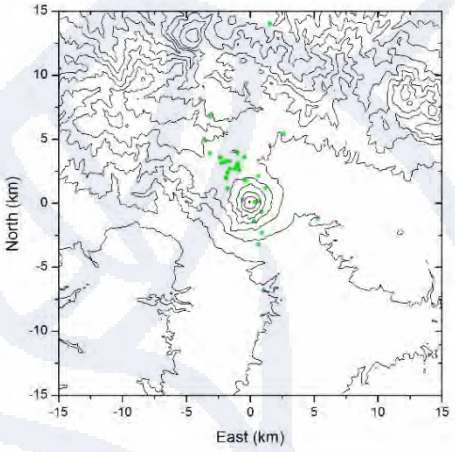

June 2013

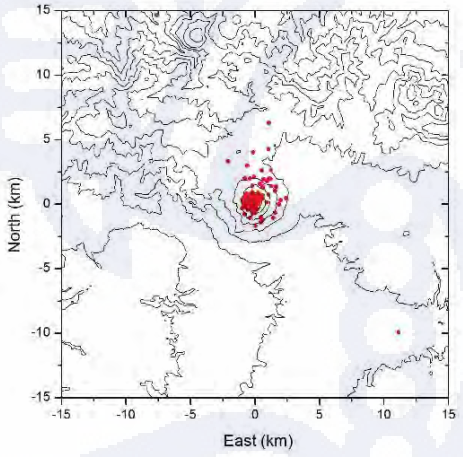

July 2013

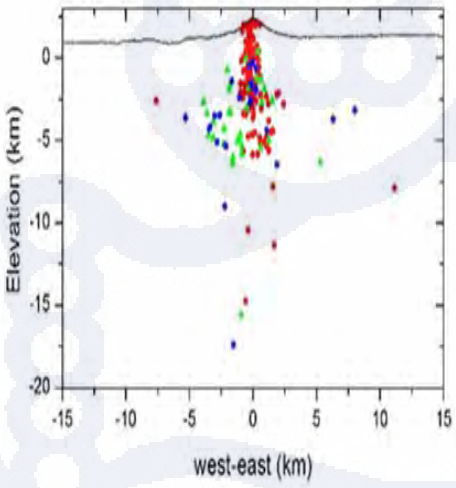

W-E cross section of VT Sinabung hypocenter

Figure III.17. The shifting of hypocenter distribution of Sinabung VT earthquakes in the period of May - July 2013. The blue circles, green triangle, and red circles are for May, June, and July 2013 hypocenters, respectively.

III.2.3 Volcano Deformation

The research uses data from Sinabung continuous GPS network to determine the rate of Sinabung volcano deformation, pressure source parameter, and calculate the volume change. The network consists of 4 permanent stations, three of them located on the slope of Sinabung volcano at distance 2.3 – 2.8 kilometers from the summit (LKWR, SKNL, and GRKI) and one station (SNBG) uses as reference is located on Sinabung volcano observatory at distance about 9 kilometer from the summit (Figure III.18).

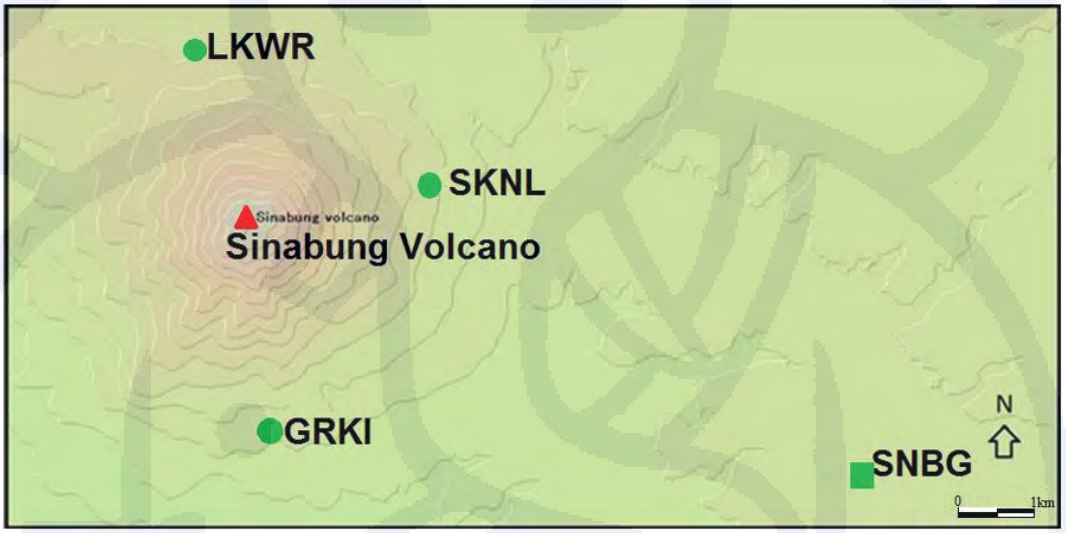

Figure III.18. Sinabung continuous GPS stations, SNBG is used as reference station for three stations in slope of the volcano.

The period of GPS data for Sinabung deformation analysis is March 2011 to October 2013. The data is observed using Leica GPS 1200 series dual frequency continuously and recorded in volcano observatory. The GPS carrier phase data were processed to obtain loosely constrained daily solutions for satellite orbits and station coordinates using the GAMIT/GLOBK software (version 10.4). The loosely constrained solutions are transformed into a consistent reference frame (ITRF 2008) to obtain the position change for each GPS observation stations. GPS solutions are analyzed using 20 IGS stations surrounding Indonesia as reference frame (BAKO, CNMR, COCO, CUSV, DARW, DGAR, GUAM, HYDE, IISC, KARR, KIT3, KOUC, KUNM, NTUS, PIMO, TNML, TOW2, TWTF, XMIS, and YAR2). To eliminate regional movement by tectonic, LKWR, SKNL, and GRKI recalculated relative to SNBG with an assumption that all observation points in Sinabung area

have the same response to regional movement and SNBG is not influenced by volcanic activity.

Horizontal Displacement

SNBG was treated as reference to detect horizontal displacements. Figure III.19 shows the time series results in ITRF 2008 relative to SNBG site. Each GPS stations (GRKI, LKWR, and SKNL) have span from 2011 to 2013. We divide the time series into three periods which separated by yellow line and red line. The period before yellow line shows very small displacement, so we assume that in this period there is no significant activity on Sinabung volcano. The data is consistent with the seismicity of the same period. Time-series show two periods of increased volcanic activity with low rate of deformation since August 2012. The horizontal displacement of Sinabung volcano during period of August 2012 – June 2013 is very small and the deformation signal is lost in the errors. The displacement after July 2013 became higher; especially in LKWR station, and after first eruption on September 15th 2013 the deformation is still continuing.

Horizontal displacements were obtained by subtracting the data between start and end time of one period after linearizing the continuous data (Table III.2). There are propagation errors for horizontal displacement in the GPS stations which amplify the error. The larger displacement is occurred in LKWR station which is located on N-NW slope of Sinabung volcano.

Table III.2. Estimation of horizontal displacement in 3 GPS stations relative to SNBG station in two periods**.**

Station	Coordinate		Horizontal Displacement (mm) August 2012 - May 2013				Horizontal Displacement (mm) June - October 2013			
	Latitude (N)	Longitude (E)	dNorth	dEast	stdNorth	stdEast	dNorth	dEast	stdNorth	stdEast
LKWR	3.192	98.385	-3.74	1.47	4.28	5.46	8.68	-7.26	6.57	6.78
GRKI	3.146	98.394	0.43	1.18	5.52	6.95	1.52	-8.05	5.39	7.37
SKNL	3.176	98.413	-3.63	1.01	2.90	4.03	3.06	-7.46	3.51	5.22

The displacement vectors of LKWR, GRKI, and SKNL sites are shown in Figure III.20. The LKWR site shows the displacement to the north-west with a greater displacement than another site. The GRKI site shows the displacement on the north-

west (dominant in west), and the SKNL site shows the displacement on the same direction with GRKI site. The displacement vectors of each station are estimated after doing differencing to SNBG site at each epoch observations

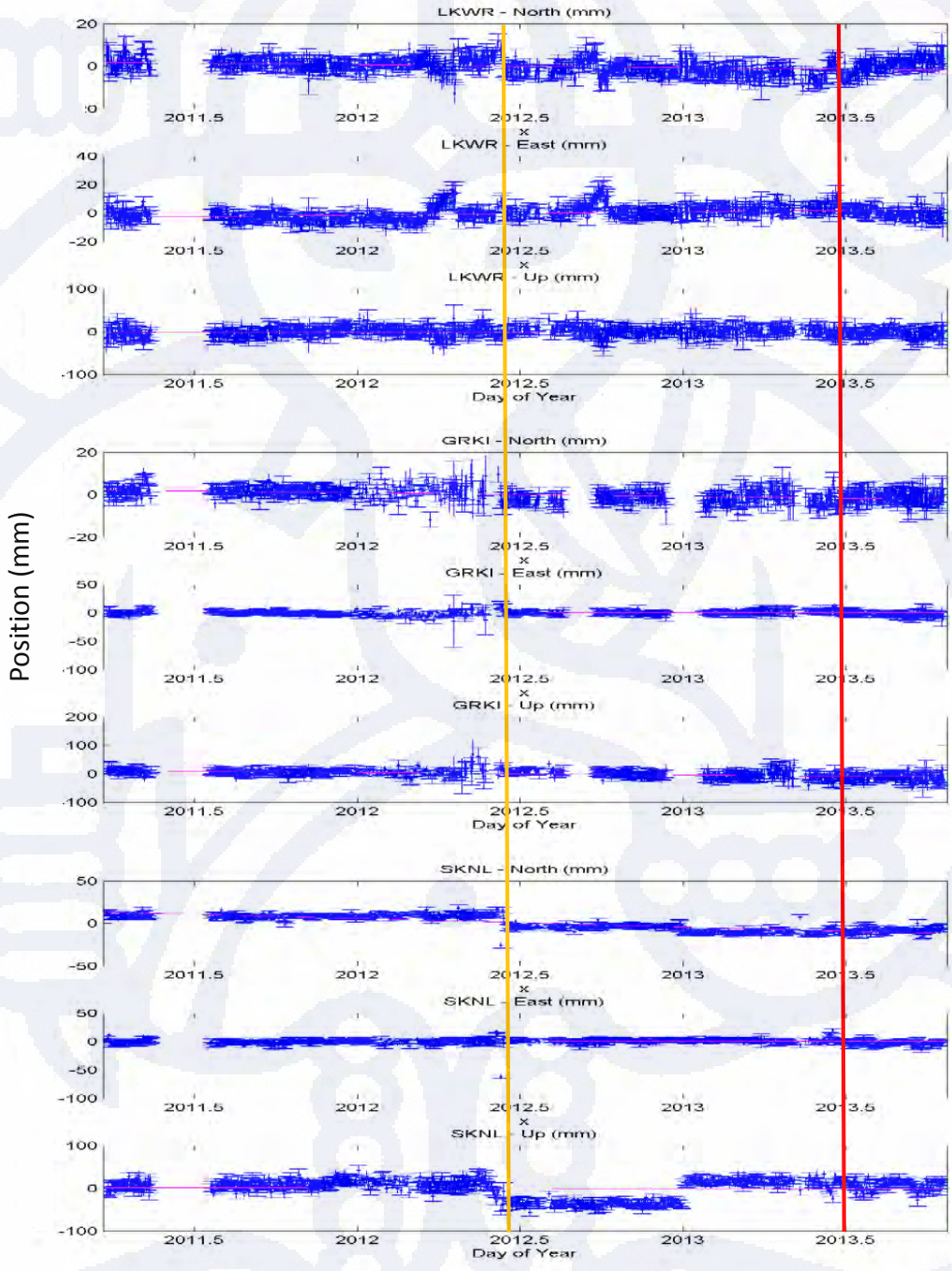

Figure III.19 The time series of GRKI, LKWR, and SKNL in ITRF 2008 relative to SNBG. The yellow line is the start of period 1 (August 2012 – June 2013) and the red line denote the start of period 2 (July – October 2013).

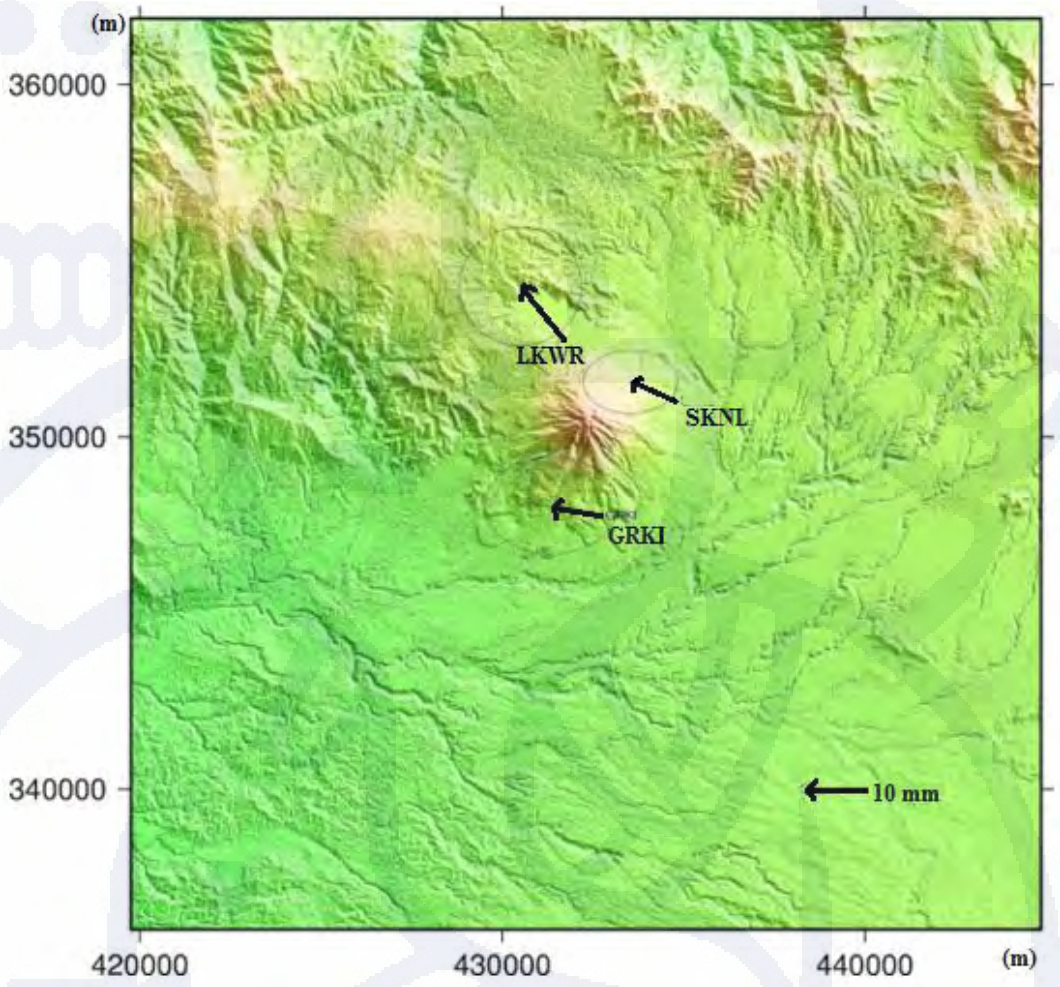

Figure III.20. Displacement vector of 3 (three) GPS stations in the slope of Sinabung volcano.

Baseline analysis

Horizontal displacements of the three stations in Sinabung slope have similar direction with slight differences in the magnitude (Figure III.20). For comparison, the baseline length between two GPS stations in the network was analyzed. The analysis use difference strategy with which is used for coordinate positioning, the network is processed without IGS stations strengthen. The 6 (six) baseline lengths are loosely constrained using GLOBK software (version 10.4), there are SNBG-SKNL, SNBG-LKWR, SNBG-GRKI, SKNL-LKWR, SKNL-GRKI, and GRKI-LKWR baselines. All baselines in Figure III.21 and Table III.3 show the positive change of baseline length in the period of July – October 2013.

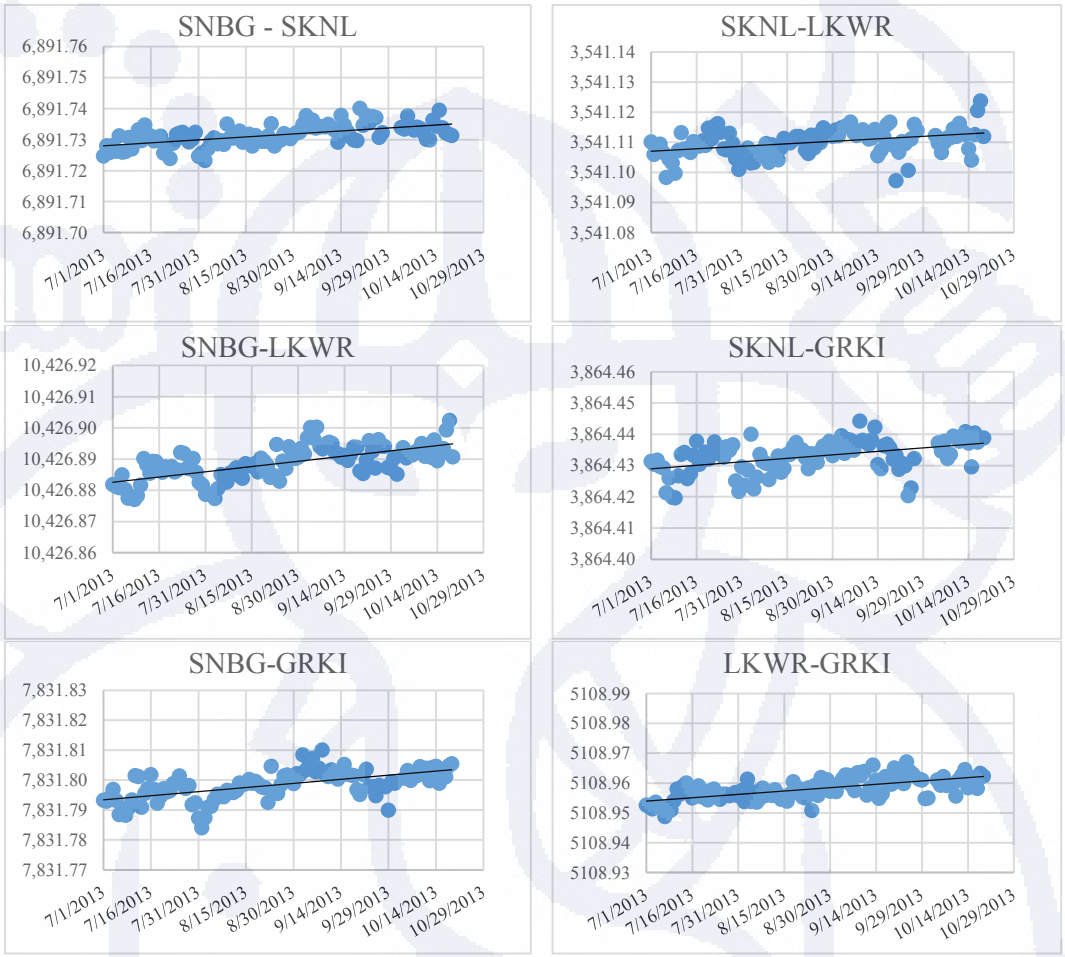

Figure III.21. Baseline between GPS stations in Sinabung volcano. Horizontal displacements were obtained by subtracting the data between start and end time of one period after linearizing the continuous data from continuous GPS network of Sinabung volcano in the period of July – October 2013. The Y-axis is baseline in meter.

Table III.3. The change of baselines length between GPS stations in Sinabung volcano in the period of July – October 2013

Baselines	dBaseline (mm)	stdBaseline (mm)
SNBG-SKNL	6.3	4.2
SNBG-LKWR	10.9	7.6
SNBG-GRKI	9.5	6.4
SKNL-LKWR	5.3	5.0
SKNL-GRKI	7.1	5.8
LKWR-GRKI	8.5	5.8

Strain Analysis

Suppose that L_{old} is distance between 2 points in unstrained state and L_{new} is in the strained one, linear strain e is defined by (Jaeger, 1962):

$$e = \frac{L_{new} - L_{old}}{L_{old}} \tag{III.3}$$

Components of horizontal strain (*exx, eyy, exy*) are defined by the equation below,

$$\begin{pmatrix} e_1 \\ e_2 \\ e_3 \end{pmatrix} = \begin{pmatrix} l_1^{\,2} & m_1^{\,2} & 2l_1m_1 \\ l_2^{\,2} & m_2^{\,2} & 2l_2m_2 \\ l_3^{\,2} & m_3^{\,2} & 2l_3m_3 \end{pmatrix} \begin{pmatrix} e_{xx} \\ e_{yy} \\ e_{xy} \end{pmatrix} \tag{III.4}$$

where

$$l_i = \cos\theta_i$$
$$m_i = \sin\theta_i$$
$$\tan\theta_i = \frac{y_2 - y_1}{x_2 - x_1}.$$

The trace of a strain tensor indicates the sum of the relative change in lengths along the coordinate axes,

$$e_{ii} = e_{xx} + e_{yy} + e_{zz}. \tag{III.5}$$

Equation (3) is linked to the volumetric change associated with deformation. When an elastic material with the volume V_0 is deformed, new volume after deformation is expressed as:

$$\frac{V}{V_0} = (1 + e_{xx})(1 + e_{yy})(1 + e_{zz}) \approx 1 + e_{ii} \tag{III.6}$$

neglecting higher-order terms.

Dilatation Θ is defined as change in volume per unit volume or sum of principal strains,

$$\Theta = \frac{\Delta V}{V_0} = e_{ii} = e_{xx} + e_{yy} + e_{zz} \tag{III.7}$$

In case of two-dimensional strain, only the horizontal axes are considered and equation (5) is simplified as,

$$\Theta = e_{xx} + e_{yy} \tag{III.8}$$

The horizontal strain in Sinabung summit is figured out by linear strain in a triangulation between LKWR, SKNL, and GRKI stations. The result of the calculation for July – October period is shown in Figure III.22. Estimated horizontal strain for July – October 2013 is 4.1 micro strain.

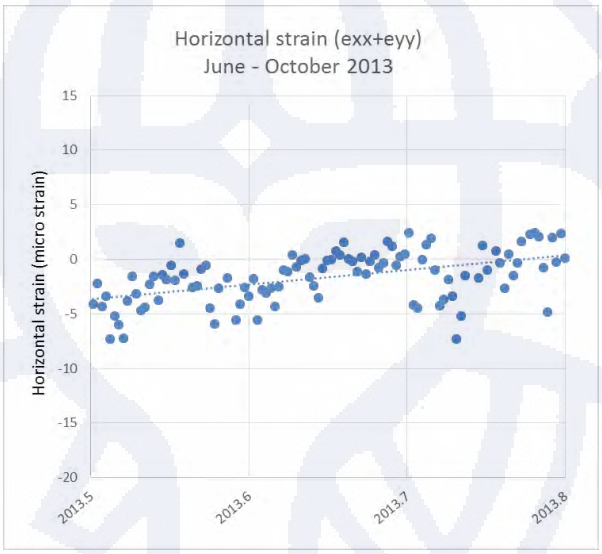

Figure III.22. Horizontal strain among three GPS stations (LKWR-SKNL-GRKI) in Sinabung volcano.

The crustal deformation of Sinabung volcano was weak before August 2012. In the period of August 2012 – May 2013 the horizontal displacement is less than 4 mm and the deformation signal is lost in the errors. The displacement after July 2013 became stronger, when the horizontal displacement is ranged 8 – 11.3 mm in the period of July – October 2013. Horizontal displacements of the three stations in Sinabung slope have similar direction with slight differences in the magnitude. Baseline analysis is done to examine the displacement between observation points and the result show positive change for all baselines. From horizontal displacement and baseline change information, the deformation of Sinabung volcano is not shown clearly. Linear strain in a triangulation between LKWR, SKNL, and GRKI stations are analyzed to determine deformation of the volcano. Horizontal strain for the triangulation shows an inflation in the summit area.

III.2.4. Sinabung volcanic Activity

Seismic data of Sinabung volcano show the September 15th 2013 eruption was preceded by:

1. The increase in VT earthquake number on July 4th 2013 with fluctuated activities since August 2010.
2. The shifting of hypocenter on July 2013 compare to several months before the increase in volcanic activity. The hypocenter move from deeper to shallower part and clustered beneath the summit until depth of 8km.

From horizontal displacement, baseline change, and horizontal strain, it can be concluded as follow:

1. Time-series shows some periods of increased volcanic activity with low rate of deformation since August 2012. Rapid deformation occurs after July 2013 and after first eruption on September 15 the inflation still continue.
2. Long period of deformation measurement shows inflation due to magmatic process beneath summit. Since no other significant precursor to the eruption, the information is important for early warning especially for volcanic activity with low rate deformation like Sinabung volcano.

The increase in VT earthquake number and inflation of Sinabung volcano occurred after the Bireun Mw6.1 earthquake of July 2, 2013. A further study is required to find out whether the deformation was triggered by the earthquake or not.